Conditions of nonstationary self-action of tightly focused high-power femtosecond laser pulse in air

Yu.E. Geints and A.A. Zemlyanov

V.E. Zuev Institute of Atmospheric Optics, Siberian Branch of the Russian Academy of Sciences, Tomsk

Received April 2, 2008

Tightly focused propagation of high-power femtosecond laser radiation in air is considered. Based on numerical solution of the nonlinear Schrödinger equation for complex envelope of light wave electric field, evolution of the beam effective radius is studied. Dependence of the rms size of a focal spot and the maximally attainable intensity of radiation at the spot focal waist on the initial laser power is established. It is shown that tight spatial focusing of ultrashort laser pulse can lead to photoionization of the medium and plasma generation in the region of maximal beam intensity. This may prevent the light wave intensity from its further growth in the focal region and retard the transversal contraction of the beam as a whole.

Introduction

Geometric focusing of laser beams or, in other words, control for the curvature of initial phase front of a light wave is traditionally used to concentrate light energy in space and to increase radiation power density. Obtaining of small, close to diffraction limit, dimensions of waist, and, simultaneously, high intensity of a light beam is of primary importance in many fields of modern science and technology, for example, laser producing of multilayer optical structures in dielectrics,[1] laser cell surgery,[2] laser scanning microscopy of living tissues,[3] and laser processing of metals and ceramics.[4] The use of laser sources, generating high-power femtosecond pulses for these purposes opens additional promises for increasing the laser beam intensity in the focal waist up to "atomic" levels ($\sim 10^{19}$ W/cm^2) at a total pulse energy of only few millijoules.[5] Advantages of just ultrashort laser action on targets include low energy ionization and ablation thresholds of materials as compared to longer laser pulses, as well as minimal thermal and mechanic damages under laser irradiation of sample regions adjacent to the zone.

High peak power and intensity of femtosecond pulses may disrupt linear focusing still before the target. In gas and condensed media, the Kerr self-focusing of radiation, multiphoton absorption, plasma formation in a medium, and other nonlinear effects lead to nonlinear changes in optical properties of the medium. Under these conditions, linear theory of diffraction of electromagnetic radiation, which gives sufficiently explicit relations between numerical aperture of the focused beam and the size of its focal spot, cannot be applied even for pre-estimates of high-power ultrashort laser pulse parameters in the region of their focusing.

Based on numerical simulation, this paper considers formation of the spatial structure of focal waist of initially tightly focused high-power femtosecond radiation under conditions of nonstationary self-action. The emphasis is made on the study of the dependence of the effective size of focal waist and maximally attainable radiation intensity of the initial power of laser radiation at the femtosecond pulse focusing in air.

Linear and nonlinear focusing of laser radiation

In case of linear propagation of laser beam, whose envelope of the electric field $E(\mathbf{r}_\perp, z)$ is described by the following Gaussian function

$$E(\mathbf{r}_\perp, z = 0) = E_0 \exp\left\{-\left|\mathbf{r}_\perp\right|^2 / 2R_0^2 + \left[i\varphi_f(\mathbf{r}_\perp)\right]\right\}, \quad (1)$$

in a medium (refractive index n_0), the radius of focal waist of the beam R_f is

$$R_f = R_0 \frac{F_0}{\sqrt{F_0^2 + k_0^2 R_0^4}} = R_0 \frac{1}{\sqrt{1 + 4/\bar{F}_0^2}}, \quad (2)$$

where $|\mathbf{r}_\perp| = \sqrt{x^2 + y^2}$ is the transversal coordinate; E_0 is the amplitude; $\varphi_f = -k_0\left(\left|\mathbf{r}_\perp\right|^2 / F_0\right)$ is the wave phase caused by the initial focusing; R_0 is the initial radius of the beam; F_0 is the initial curvature radius of the wave phase front; $k_0 = 2\pi n_0/\lambda_0$ is the wave number; λ_0 is the wavelength in vacuum. The waist itself has the center at a point $\bar{z}_f = 4\bar{F}_0/(\bar{F}_0^2 + 4)$ (linear focus) and the characteristic length $\bar{L}_f = 4(R_f/R_0)^2$. Hereinafter in the text, for convenience we normalize dimensional parameters to the Rayleigh length $L_R = k_0 R_0^2/2$: $\bar{z}_f = z_f/L_R$, $\bar{f}_0 = F_0/L_R$.

The radiation wavelength λ_0 is a natural restriction on the extension of the focal waist. According to Eq. (2), we can estimate the attainable radius of the focal spot[6] as $R_f^* \approx \lambda_0/2$.

0235-6880/08/09 688-09 $02.00

At the beam focusing, the average (over the cross section) radiation intensity in the focal spot $\bar{I}_f = P_0/(\pi R_f^2)$ ($P_0 = cn_0/(8\pi)\int|E|^2\,d\mathbf{r}_\perp$ is the initial power of radiation) increases as compared to the initial value of $\bar{I}_0$ proportionally to the square of the reciprocal natural (diffraction) angular divergence θ_d:

$$\mu_f = \frac{\langle I_f \rangle}{\langle \bar{I}_0 \rangle} = 1 + \frac{R_0^2}{F_0^2\theta_d^2}; \quad \theta_d = \frac{1}{k_0 R_0}. \qquad (3)$$

In a medium with cubic optical nonlinearity of the Kerr type, the light beam propagation has a self-action character. The polarizability of molecules and, consequently, the refractive index of such a medium begin to depend on the optical field intensity $n(I) = n_0 + n_2 I$, where the parameter n_2 characterizes the optical strength of the Kerr effect. This leads to the light wave self-focusing. According to the self-focusing theory,[7] if the beam power is higher than some threshold value P_c, being the critical power of the self-focusing, then, due to the Kerr effect, the beam experiences transversal collapse (contraction to a point) at a distance $\bar{z}_K = 1/\sqrt{\eta - 1}$, where $\eta = P_0/P_c$. The value of P_c is determined by a nonlinear addition to the refractive index of the medium n_2 and can be expressed as $P_c = \lambda_0^2/(2\pi n_2)$. It is obvious that at $\eta = 1$ for collimated radiation the nonlinear Kerr lens compensates natural blooming of the beam.

In terms of linear optics, the action of the Kerr effect is equivalent to focusing of the light beam by a spherical lens with the focal length dependent on the beam power. If the laser beam is initially focused at the point z_f and propagates through a Kerr medium, then the resultant position of its nonlinear focus z_N is determined by the joint action of the initial and induced focusing:

$$z_N = z_K F_0/(z_K + F_0). \qquad (4)$$

Estimates of focusing characteristics of a beam in a Kerr medium based on equations of the theory of stationary self-focusing[7] suggest that radiation can be focused to a spot with size even smaller than the diffraction limit, which would allow obtaining ultrahigh intensities of the optical field in an extremely small volume of a medium.[8] However, as it will be shown below, this effect is not actually observed, because mechanisms preventing further self-contraction of the beam always take place in a medium at high intensities. Most significant of these mechanisms in gaseous and condensed media are photoionization and plasma formation in the beam channel.

The Drude–Lorentz model of the free-electron gas[9] gives the variation of the complex refractive index of a medium $m = n + i\kappa$ upon its photoionization as

$$m_p = -\frac{\omega_p^2\tau_c^2}{2n_0\left(\omega^2\tau_c^2 + 1\right)}\left(1 - \frac{i}{\omega\tau_c}\right), \qquad (5)$$

where $\omega_p = \sqrt{e^2\rho_e/(m_e \in_0)}$ is the plasma frequency; ρ_e is the concentration of free electrons (plasma density); τ_c is the characteristic time of collision of free electrons with heavy particles; e and m_e are the electron charge and mass; ω is the frequency of the light wave; $\in_0$ is the universal electric constant. As can be seen from Eq. (5), the influence of plasma nonlinearity on the optical field manifests itself both in the change of the wave phase (real part of m_p), leading to wave defocusing, and in the decrease of the field energy (imaginary part of m_p) due to photon absorption by free electrons through the mechanism inverse to the deceleration emission. In this case, $|m_p|$ is proportional to the instantaneous plasma density ρ_e.

The instantaneous concentration of free electrons in the medium can be determined from the rate equation taking into account the multiphoton and cascade mechanisms of ionization, as well as the decrease in the electron concentration due to their recombination with ions:

$$\frac{\partial\rho_e}{\partial t} = W_I(I)(\rho_{nt} - \rho_e) + \frac{\sigma_c}{n_0\Delta E_i}\rho_e I - \nu_r\rho_e^2, \qquad (6)$$

where $W_I(I)$ is the variable (with intensity) photoionization rate of the medium; ρ_{nt} is the density of neutral atoms (molecules);

$$\sigma_c = \omega_p^2\tau_c\Big/\left[c\rho_e\left(\omega^2\tau_c^2 + 1\right)\right];$$

ΔE_i is the cross section of the cascade ionization and the ionization potential of a molecule, respectively; ν_r is the recombination rate. As high-power femtosecond laser pulses propagate in a gas, two last terms in the right-hand side of Eq. (6) appear to be insignificant as compared to the first term. Therefore, they are usually neglected in particular estimates of the laser plasma density.

The photoionization of molecules leads to additional absorption of the radiation energy in the medium. The nonlinear absorption coefficient of the medium α_I associated with this process has the form

$$\alpha_I = \frac{W_I(I)}{I}\Delta E_i(\rho_{nt} - \rho_e).$$

Then the total absorption coefficient of the wave energy at plasma formation in a gas can be determined taking into account Eqs. (5) and (6):

$$\alpha_N = \alpha_p + \alpha_I = \sigma_c\rho_e + \frac{W_I(I)}{I}\Delta E_i(\rho_{nt} - \rho_e), \qquad (7)$$

where $\alpha_p = \mathrm{Im}(m_p)$. The energy loss of radiation manifests itself, first of all, in the decrease of the instantaneous pulse intensity. Therefore, the focusing effect of the Kerr nonlinearity decreases as well.

Thus, at spatial focusing of an ultrashort laser pulse, one should take into account not only the appearance of the nonlinear Kerr lens, but also the inverse effect of plasma nonlinearity on a light wave.

It should be noted that at high radiation intensities, the medium hyper-polarizability may appear due to five-order nonlinear susceptibility in terms of the field $\chi^{(5)}$. In this case, the refractive index can be represented as a sum of three terms: $n(I) = n_0 + n_2 I - n_4 I^2$. As is seen, the nonlinear addition n_4 decreases the focusing action of the Kerr effect by the saturation mechanism:

$$n_2(I) = n_2 - n_4 I \simeq n_2/(1 + I/I_{\text{sat}}),$$

where $I_{\text{sat}} = n_2/n_4$ is the characteristic intensity of the saturation.[10] It is obvious that the particular role of the five-order nonlinearity in the process of radiation self-focusing is determined by the relation between characteristic intensities of saturation and plasma formation, which, in their turn, depend on optical characteristics of the medium itself. For example, for atmospheric air at $\lambda = 800$ nm, according to Ref. 11, $n_2 = 3.2 \cdot 10^{-19}$ cm^2/W, $n_4 = 2.5 \cdot 10^{-33}$ cm^4/W^2, while the saturation intensity is $I_{\text{sat}} = 10^{14}$ W/cm^2. In this case, active plasma formation in air, as numerical calculations show (see Ref. 12), starts already at pulse intensity $I \sim 10^{13}$ W/cm^2. This fact allows us to ignore hyper-polarizability of the medium in future.

Numerical model of radiation propagation

As a mathematical basis for simulation of ultrashort radiation focusing in gas, we used the formalism of the nonlinear Schrödinger equation (NSE) written for the slowly varying complex amplitude of a light pulse electromagnetic field $U(\mathbf{r}_\perp, z; t) = E/E_0$. This equation takes into consideration not only beam diffraction and frequency dispersion of air, but also some nonlinear effects responsible for amplitude and phase self-modulation of the light wave (see, for example, Ref. 13). Let us write NSE in the following form:

$$\left\{\frac{\partial}{\partial z} - \frac{i}{2n_0 k_0}\nabla_\perp^2 + i\frac{k_\omega''}{2}\frac{\partial^2}{\partial t^2}\right\}U(\mathbf{r}_\perp, z; t) - ik_0(\tilde{n}_2 - n_{\text{p}}) \times$$

$$\times U(\mathbf{r}_\perp, z; t) + \frac{\alpha_N}{2}U(\mathbf{r}_\perp, z; t) = 0, \qquad (8)$$

where

$$n_{\text{p}} = \text{Re}(m_{\text{p}}); \quad k_\omega'' = \partial^2 k/\partial\omega^2$$

is the dispersion of group velocity of the light pulse in air (0.21 fs^2/cm at λ = 800 nm);

$$\tilde{n}_2 = \frac{n_2}{2}\left\{(1-\beta)|U|^2 + \beta\int_{-\infty}^{t} dt'\Lambda(t-t')|U(t')|^2\right\}$$

is the cubic nonlinearity of the refractive index taking into account the instantaneous and lagger components of the Kerr effect; β is the specific fraction of the lagged Kerr effect. The nonlinear absorption coefficient of the medium α_N is taken into account through Eq. (7).

The lagger component in the Kerr effect is connected with the finite time of orientation of anisotropic molecules along the electric field vector. This lagged character of the response was taken into account within the framework of the decaying oscillator model[14]:

$$\Lambda(t) = \theta(t)\Omega_{\text{R}}\exp(-t/\tau_{\text{d}})\sin\Omega_{\text{R}}t,$$

where Ω_{R} is the frequency, and τ_{d} is the characteristic decay of molecular vibrations (for air $\Omega_{\text{R}} \simeq 20$ THz, $\tau_{\text{d}} \simeq 70$ ns); $\theta(t)$ is the Heavyside function.

The numerical integration of NSE (8) was performed using the technique of division of the initial problem at each step over the evolutional variable z into two problems: nonlinear one, in which formation of the induced phase of the field is calculated, and linear one, in which the field amplitude is transformed as a result of diffraction and dispersion of the wave packet with the phase front determined at the previous step. To improve the stability of computations, we used the combination of the Fourier spectral method (in time), the implicit three-level difference scheme of the Crank–Nicholson type (in transversal coordinates), and the adaptive correction of the grid step in the evolutional variable. The concentration of free electrons ρ_{e} was determined through solution of Eq. (6) by the Runge–Kutta method.

Model of photoionization of a gas medium

As a model of photoionization of air, we used the Perelomov–Popov–Terent'ev (PPT) model,[15] which, as was stated in Ref. 16, most completely describes the available experimental data. According to the PPT model, the photoionization rate $W_l(I)$ of the level with the bond energy ΔE_{i}, orbital moment l, and its projection j to the field direction has the form

$$W_l(I) = \frac{\Delta E_{\text{i}}}{\hbar}|C_{\text{nl}}|^2 f_{lj}\sqrt{\frac{6}{\pi}}\left(\frac{2E_{\text{a}}}{E}\right)^{2n^*-3/2} \times$$

$$\times(1+\gamma^2)^{3/4}A_j(\gamma)\exp\left(-\frac{2E_{\text{a}}}{3E}g(\gamma)\right), \qquad (9)$$

where $\gamma = \frac{\omega_0}{c}\sqrt{\frac{c\,\epsilon_0\,m_{\text{e}}\Delta E_{\text{i}}}{I}}$ is the Keldysh parameter; $E_{\text{a}} = 10^5$ V/m is the strength of the intra-atomic field;

$$|C_{\text{nl}}|^2 = \frac{2^{4n^*-2}}{n^*\Gamma(n^*+l+1)\Gamma(n^*-l)}$$

is the constant. Here $n^* = Z\sqrt{\Delta E_H/\Delta E_i}$ is the effective main quantum number; Z is the charge of the atomic residue; ΔE_H is the ionization energy of the hydrogen atom; Γ is the gamma function. Other coefficients have the following form:

$$g(\gamma) = \frac{2}{3\gamma}\left[\left(1+\frac{1}{2\gamma^2}\right)\mathrm{arcsinh}(\gamma) - \frac{\sqrt{1+\gamma^2}}{2\gamma}\right];$$

$$f_{lj} = \frac{(2l+1)(l+|j|)!}{2^{|j|}|j|!(l-|j|)!},$$

$$A_j(\gamma) = \frac{4}{\sqrt{3}\pi}\frac{1}{|j|!}\frac{\gamma^2}{1+\gamma^2}\sum_{n\geq m_i}^{\infty}\exp\left(-\alpha(n-m_i)\right)W_j\left(\beta\sqrt{n-m_i}\right),$$

$$\alpha = 2\left[\mathrm{arcsinh}(\gamma) - \frac{\gamma}{1+\gamma^2}\right],\quad \beta = \frac{2\gamma}{\sqrt{1+\gamma^2}},$$

$$W_j(x) = \mathrm{e}^{-x^2}\int_0^x \mathrm{e}^{-y^2}(x^2-y^2)^{|j|}!\,\mathrm{d}y.$$

In practice, the use of Eq. (9) for calculation of the ionization rate is not always convenient in the NSE numerical simulation, since it requires calculation of many coefficients at every step as the wave intensity changes. Therefore, for faster computations, we approximated the dependence $W_I(I)$, described by Eq. (9), by the function $W_I(I) = A_W(I)I^K$, where the coefficients A_W and K are selected according to the medium type and laser radiation wavelength. Thus, for atmospheric gases, we obtained the functional dependence of the form

$$\log\left(A_W(I)\right) = \log(A_0) - A_1\exp\left(-\frac{\log^2(I/I_c)}{A_2^2}\right) =$$

$$= \log(A_0) - A_1\exp\left(-\frac{1}{A_2^2}\log^2\left[\frac{I_0}{I_c}|U|^2\right]\right),$$

where

for O_2: $K = 7.44$; $A_0 = 10^{-119.378}\ \mathrm{s}^{-1}\,(\mathrm{m}^2/\mathrm{W})^K$; $A_1 = 13.445$; $A_2 = 2.041$; $I_c = 10^{20.616}\ \mathrm{W/m}^2$,

for N_2: $K = 10.165$; $A_0 = 10^{-168.530}\ \mathrm{s}^{-1}\,(\mathrm{m}^2/\mathrm{W})^K$; $A_1 = 19.223$; $A_2 = 2.012$; $I_c = 10^{20.688}\ \mathrm{W/m}^2$.

Structure of nonlinear focus of ultrashort pulse

Consider the evolution of parameters of high-power femtosecond radiation during its focused propagation in air. For definiteness, we reproduce numerically the experimental conditions from Ref. 17. So, the initial form of the normalized envelope of the radiation electric field (Gaussian in time and space)

$$U(\mathbf{r}_\perp, z, t) = \mathrm{e}^{-\left(|\mathbf{r}_\perp|^2/2R_0^2\right)+i\varphi_f(\mathbf{r}_\perp)-\left(t^2/2t_p^2\right)}$$

is specified in calculations by the following parameters: pulse duration $t_p = 60$ fs, beam radius $R_0 = 2.8$ mm (by $1/e$ level of the maximal intensity), and a wavelength of 800 nm. The initial curvature radius of the radiation phase front was taken equal to 86 cm, therefore, its normalized value was $\bar{F}_0 = F_0/L_R = 0.028$ ($L_R = 30.8$ m).

When specifying the initial radiation energy, two versions were first considered: subcritical radiation power ($\eta = 0.1$, $P_c = 3.2\ \mathrm{GW/cm}^2$) and the seven-fold excess of its peak power P_0 above the critical level P_c ($\eta = 7$). Thus, we had the initial peak pulse intensity $I_0 = 1.3\cdot 10^9$ and $9\cdot 10^{10}\ \mathrm{W/cm}^2$ in the first and second cases, respectively. The position of the nonlinear focus of the beam (4) at $\eta = 7$ can be estimated as $z_K = 13$ m, $z_N = 81$ cm, that is, the Kerr effect under these conditions only insignificantly shifts the focal waist of the beam from its position in the linear medium.

Figure 1 shows the dependence of the laser beam transversal dimension on the longitudinal coordinate. In calculations, equation (8) was used. Figure 1 demonstrates variation of two parameters: the geometric size R_1 determined from the beam energy density profile $w(\mathbf{r}_\perp, z) = \int_{-\infty}^{\infty} I(\mathbf{r}_\perp, z; t')\mathrm{d}t'$ at the level $1/e$ of the maximum and the effective radius R_e, which is calculated as a normalized second-order moment of the wave intensity[18]:

$$R_e(z) = \left[\frac{1}{W(z)}\int_{-\infty}^{\infty}\mathrm{d}t'\iint_{\mathbf{R}_\perp}\mathrm{d}^2\mathbf{r}_\perp I(\mathbf{r}_\perp, z; t')\left|(\mathbf{r}_\perp - \mathbf{r}_{gr})\right|^2\right]^{1/2}, \quad (10)$$

where $\mathbf{r}_{gr}$ is the radius vector of the beam centroid:

$$\mathbf{r}_{gr} = \frac{1}{W(z)}\int_{-\infty}^{\infty}\mathrm{d}t'\iint_{\mathbf{R}_\perp}\mathrm{d}^2\mathbf{r}_\perp\cdot\mathbf{r}_\perp I(\mathbf{r}_\perp, z; t');$$

W is the total energy of the pulse. It should be noted that this parameter is useful in analysis of complex beam intensity profiles, because, according to its definition, the effective radius indicates the size of the spatial area, in which no less than 50% of the total beam energy is concentrated. For the Gaussian transversal intensity profile, the geometric R_1 and effective R_e radii have the same value.

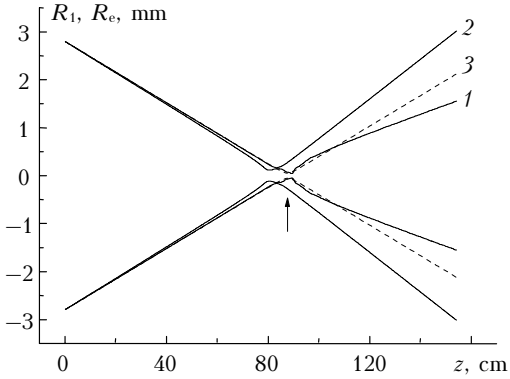

Fig. 1. Geometric (curves *1* and *3*) and effective (*2*) radii of tightly focused femtosecond beam as functions of the longitudinal coordinate at the relative initial pulse power $\eta = 7$ (*1*, *2*) and 0.1 (*3*). Vertical arrow shows the position of the geometric focus.

It is seen in Fig. 1 that the focused beam propagates under linear and nonlinear conditions in different ways. At the above-critical initial pulse power, ($\eta = 7$), R_1 and R_e differ widely starting already from the distance $z \simeq 40$ cm. Then, in the region of the focal waist ($z \geq 80$ cm), an extended axial structure – light filament – is formed. This difference is connected with the action of Kerr nonlinearity, which makes sharper the initially Gaussian beam profile and thus decreases its geometric size, but does not affect significantly the pulse energy redistribution over the beam cross section.

In contrast to the geometric radius R_1, evolution of the effective radius R_e during focusing the beam of above-critical power demonstrates a pronounced waist with a center at $z_g \simeq 84$ cm. It is important to note that the effective radius of the tightly focused beam under both linear and nonlinear conditions evolves similarly up to the *global* nonlinear focus z_g, which is formed earlier than the geometric one under self-focusing.

The first minimum in the dependence of the geometric radius $R_1(z)$ appears at the point of the *local* nonlinear focus $z = z_N$ and amounts to $R_1(z_N) \simeq 114$ μm, which is nearly by three times wider than the radius of the beam focal waist at linear propagation: $R_f = 43$ μm. This is caused by the processes of air ionization and plasma formation, which prevent the further contraction of the beam, forming, along with the Kerr effect, a light filament at the axis with the quasiconstant peak intensity $I_m \approx 4 \cdot 10^{13}$ W/cm^2. The transversal radius of this structure is not, however, constant. It pulses, reaching the absolute minimum $R_1 \simeq R_f$ at the point $z \simeq 89$ cm. Then the beam begins to stably diverge.

Consider the stages of formation of the focal waist of ultrashort pulse in more detail. To do this, introduce an additional dimensional beam parameter – an instantaneous effective radius R_{et}, whose square is determined by

$$R_{et}^2(z,t) = \frac{1}{P(z,t)} \iint_{\mathbf{R}_\perp} d^2\mathbf{r}_\perp I(\mathbf{r}_\perp, z; t') \left| \left(\mathbf{r}_\perp - \mathbf{r}_{gr}^t\right) \right|^2 \quad (11)$$

at

$$\mathbf{r}_{gr}^t = \frac{1}{P(z,t)} \iint_{\mathbf{R}_\perp} d^2\mathbf{r}_\perp \cdot \mathbf{r}_\perp I(\mathbf{r}_\perp, z; t').$$

As is seen, this parameter determines the effective size of every individual "temporal cross section" of the pulse and is related to the time-integral effective radius (10) through the obvious relationship

$$R_e^2(z) = \left[\int_{-\infty}^{\infty} P(z,t)\, dt \right]^{-1} \int_{-\infty}^{\infty} P(z,t) R_{et}^2(z;t)\, dt. \quad (12)$$

The evolution of R_{et} along the path is shown in Fig. 2*a*. The curves correspond to different instants within the pulse duration, whose particular positions are numbered in Fig. 2*b*.

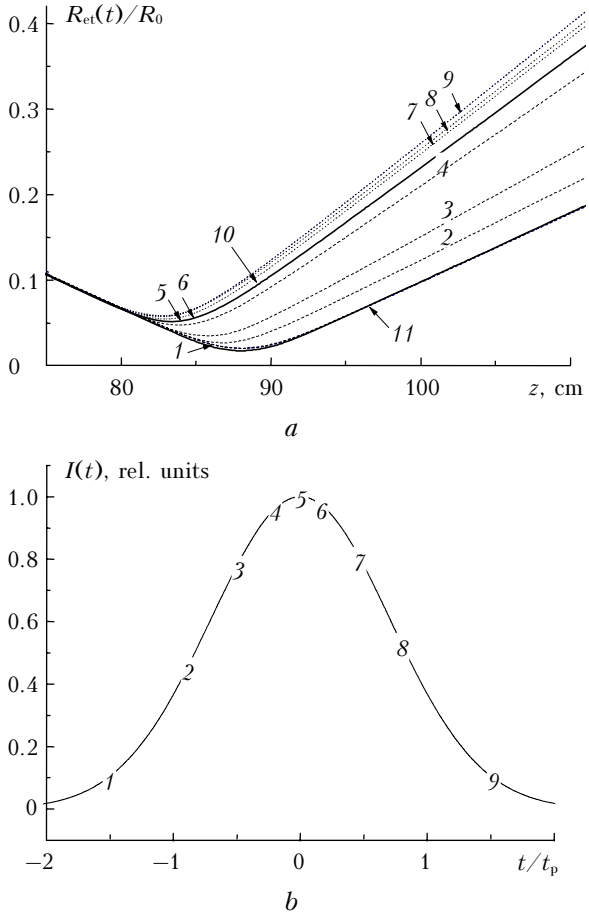

Fig. 2. Evolution of the temporal effective radius R_{et} of the focused femtosecond pulse with the initial intensity $\eta = 7$ (*a*) and time profile of the relative pulse intensity (*b*). Curve numbers in Fig. 2*a* correspond to time pulse cross sections shown in Fig. 2*b*.

Thus, curves *1–3* give the effective radius of time cross sections for the leading front of the pulse, curves *7–9* give it for the trailing front of the pulse, and the size of the profile cross sections at points *4–6* corresponds to the central part of the laser pulse. This figure also shows the evolution of the integral effective radius R_e at nonlinear and linear (curves *10* and *11*) propagation of the beam.

Analysis of Fig. 2 shows that all time cross sections of the pulse evolve identically up to a certain point of the path ($z \simeq z_N$). Then each of them forms a focal waist, whose position at the path z_{ft} and the transversal radius $R_{etf} = R_{et}(z_{ft})$ depends on the position of every cross section in the pulse. The leading front of the pulse (curve *1*), having the sub-critical power, practically does not induce the medium nonlinearity during propagation, and the law of evolution of its spatial radius is the same as in the linear case (curve *11*). The higher is the instantaneous power (curves *2–4*), the stronger is the effect of the Kerr self-focusing. Since the density of free electrons at every point of the path increases with time upon photoionization of the gas [see Eq. (6)], the following (in time) pulse levels experience a stronger

compensating action of the plasma nonlinearity. This increases the focal waist size in every following time level, making its center closer to the path beginning. As a result, in place of one focal spot localized at a point, known from linear optics, an extended waist of variable diameter is formed upon focusing of a high-power femtosecond pulse. This waist consists of many focal spots corresponding to different time pulse layers. Time layers lying at the leading front of the pulse have the smallest radius R_{etf} in the point z_{ft} of its focus, while layers lying at the trailing front have the largest radius (Fig. 3).

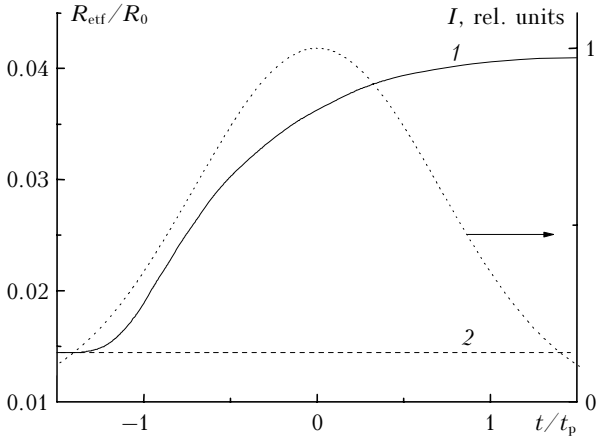

Fig. 3. Transversal radius of the focal waist of the femtosecond pulse: effective radius of the focal waist R_{et} of every time layer as a function of its position in the pulse (*1*); waist radius at linear focusing of radiation (*2*). Time profile of the pulse is shown by a dashed curve.

The considered physical pattern of the layer-by-layer self-focusing of an ultrashort light pulse is in qualitative agreement with the model of dynamic moving focuses (DMF), which was initially proposed in Refs. 19 and 20 and then modified for ionized medium and focused beams in Refs. 21 and 22. In this theoretical model, a light filament is treated as a series of local focuses of different time pulse layers appeared at a different distances from the beginning of the optical path. The transversal size of the filament at every point is equal to the size of the corresponding focal spot. A consequence of the DMF model and, at the same time, its limitation is the fact that for a pre-focused beam the formed filament cannot go beyond the beam geometric focus, while experiments and numerical calculations (see, for example, Fig. 1) contradict this statement.

This contradiction can be resolved, if to analyze the beam self-focusing in terms of effective parameters. In this case, as it is seen from Fig. 2*a*, the position of the focal waist of the instantaneous effective radius, which bounds the spatial area of localization of the instantaneous power of every temporal beam layer, always does lie to the left from the point of the beam geometric focus z_f (minimum of curve *11*). From this point of view, the DMF model does not contradict the physical pattern of the considered phenomenon and can be used for qualitative interpretation of nonstationary self-focusing of tightly focused radiation as well.

The effective beam radius being integral over the whole temporal profile of the beam (*global* effective radius), indicates the zone, in which the most part of radiation energy is localized. Therefore, the evolution of R_e almost fully copies the evolution of the instantaneous radius R_{et} of the pulse central part (curves *5*, *6*, and *10* in Fig. 2*a* merge together). It should be also noted that the output angle of the effective radius of every temporal cross section at the focal point exceeds the corresponding input angle and monotonically increases to the pulse end due to the increasing action of the plasma nonlinearity (refraction and absorption).

Of interest is the maximally achievable level of the pulse intensity at the focal waist of a femtosecond beam at variation of its power. According to Eq. (3), for conditions of numerical experiment at linear focusing of the beam with $\bar{F}_0 = 0.028$, we have the calculated degree of intensity growth $\mu_f = 5102$. This value of relative intensity, as is seen from Fig. 4, is achieved only at an essential sub-critical pulse power ($\eta \le 0.1$).

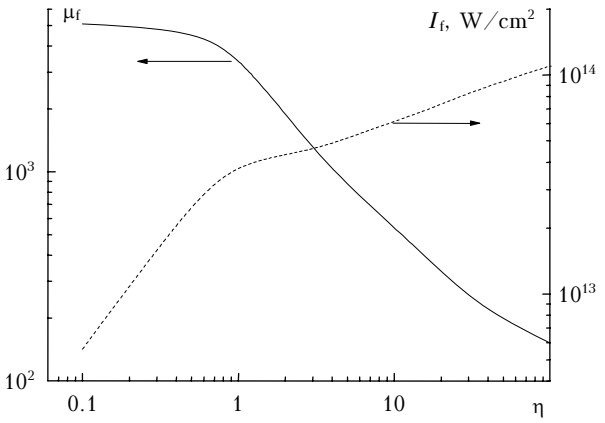

Fig. 4. Degree of intensity growth μ_f at focal waist of a femtosecond pulse and maximally achievable intensity I_f as a functions of η.

The increase of the initial power of radiation first leads to the slow decrease of μ_f in the range of moderate power values ($\eta = 0.5 \div 1$). With further growth of η, the relative intensity at the focus decreases almost by the linear law.

The coordinate of the path point z^*, at which the pulse intensity reaches its maximum, is shown in Fig. 5.

It is seen that when focusing radiation of sub-critical power, the maximum lies exactly in the center of the linear focal waist $z_f = 85.9$ cm. With the further growth of the pulse power, the point of maximal intensity approaches the path beginning and the inequality $z^* \simeq z_g$ always holds. In other words, as a femtosecond pulse is focused, the maximal radiation intensity is gained near the *global* rather than local focus of the beam. The local focus z_N indicates only the beginning of the light filament.

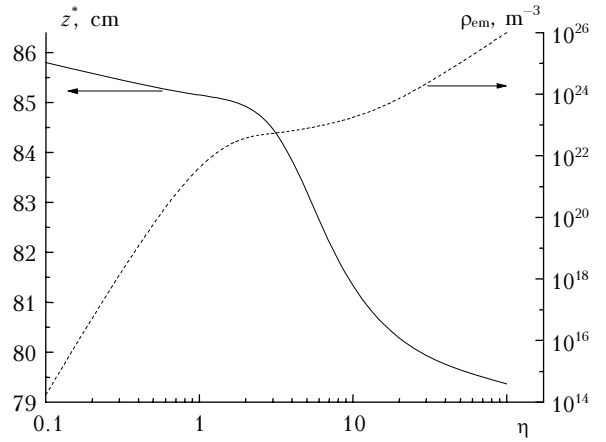

Fig. 5. Coordinate of the global maximum of the pulse intensity z^* and the maximal concentration of free electrons ρ_{em} as functions of η.

Consider absolute values of the maximal intensity, which take place in the beam focus zone (see Fig. 4, dashed curve). A break in the dependence $I_f(\eta)$, clearly seen in Fig. 4, corresponds to changes of beam focusing conditions, which take place when the intensity at the focus I_f achieves a value of $2–4 \cdot 10^{13}$ W/cm^2. In this case, as was noted above, the plasma nonlinearity begins to prevent markedly (through variation of the complex refractive index [see Eq. (5)] the further growth of the beam intensity at the Kerr self-focusing.

As the result of the competitive action of these two processes, dynamic balance is established in each time cross section of the pulse, at which the peak amplitude of the light wave becomes limited. If at the leading front of the pulse the limitation of the peak intensity is connected with the use of the wave energy for the gas photoionization (imaginary part of m_p), then at the center and at the trailing front of the pulse the refractive action of the already formed plasma dominates (real part of m_p).

The calculations show (Fig. 5, dashed curve), that the maximal concentration of free electrons in the beam channel ρ_{em}, at which focusing conditions alternate, corresponds to $\rho_{em} \sim 10^{23}$ m^{-3}.

At essentially above-critical level of the beam power ($\eta \gg 1$), the continuing growth of the peak intensity at the nonlinear focus also increases the density of the forming plasma, thus increasing ρ_{em} up to the level ~10^{26} m^{-3}, which is already close to the equilibrium concentration of neutral nitrogen molecules in air (according to the conditions of numerical experiment $\rho_{nt} \sim 1.2 \cdot 10^{26}$ m^{-3}). This is indicative of high, close to unity, degree of medium ionization by radiation and possible occurrence of optical breakdown in air, when the conditions for electron avalanche take place in the beam channel (according to Ref. 9, breakdown threshold for atmospheric air is $\sim 2 \cdot 10^{14}$ W/cm^2). The further increase of the initial power of radiation already is not efficient from the viewpoint of increase of the peak intensity at the global focus of the beam, since the optical breakdown plasma, formed at the leading front of the pulse, blocks the propagation of the rest of the pulse.

Introduce another effective parameter characterizing propagation of the ultrashort pulse, namely, effective intensity I_e, which is defined as follows:

$$I_e(z) = \frac{E(z)}{\pi^{3/2} t_{pe}(z) R_e^2(z)} .$$

Here

$$t_{pe} = \left[\frac{1}{E(z)} \iint\limits_{\mathbf{R}_\perp} d^2\mathbf{r}_\perp \int\limits_{-\infty}^{\infty} dt' I(\mathbf{r}_\perp, z; t') t'^2 \right]^{1/2}$$

is the rms pulse duration. According to this definition, for the Gaussian (in space and time) pulse in the linear medium, the effective radiation intensity $I_e(z)$ at every point of the path is equal to the peak value of the real intensity. The ratio $\mu_e = I_e(z)/I_0$ along the propagation path for focused beams of the different initial power is shown in Fig. 6.

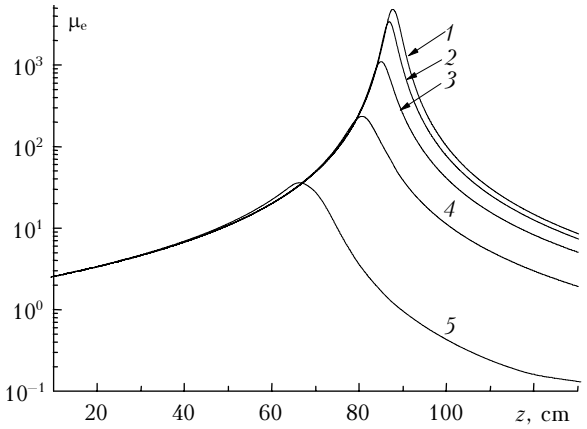

Fig. 6. Relative efficient intensity of laser radiation μ_e as a function of propagation distance z at different initial relative pulse powers: η = 0.1 (*1*), 1 (*2*), 3 (*3*), 15 (*4*), and 100 (*5*).

It is seen how nonstationary self-action of radiation changes the dynamics of beam focusing, resulting in the shift of its global focal waist and the decrease in the maximum average intensity at the global focus.

Figure 7 shows the effective radius of the focal waist $R_{ef} = R_e(z = z_g)$ formed at spatial radiation focusing of the femtosecond beam of different initial powers. This figure shows that under conditions of significantly nonlinear radiation propagation ($\eta > 1$) the focusing of a pulse to the level of the diffraction limit, predicted in the linear theory, becomes *impossible* [see Eq. (2)].

It should be emphasized that here we deal the effective integral size of the focal waist (12) calculated as a focal radius of every time layer of the pulse, averaged over the temporal power profile. This radius characterizes the size of the area of the pulse energy localization, and may differ from an instantaneous value of the beam radius, determined from the energy

profile. As was noted above (Fig. 3), this size has the minimal, diffraction-limited value in the zone of low intensity at the pulse leading front. Just this fact can likely explain the extremely small size of the focal spot (2–3 μm) in diameter, observed experimentally in Ref. 5 at focusing femtosecond pulses of the Ti:sapphire laser in air. Initial peak power in pulses was $\sim 10^{14} - 10^{17}$ W/cm^2 and, consequently, initially exceeded the breakdown threshold of air. In other words, based on the above results, the diffraction-limited (minimal) value of the effective transversal dimension of the focal waist of an ultra-short high-power pulse can be formed only at the leading front of the pulse, where the density of the formed plasma is still low and, correspondingly, its defocusing action on radiation is weak.

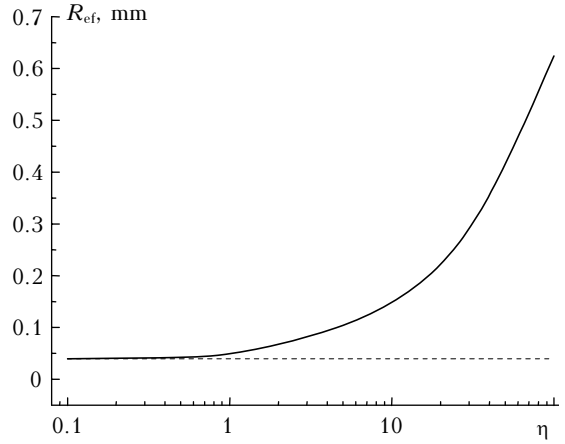

Fig. 7. Effective radius of focal waist of the femtosecond beam R_{ef} as a function of the initial radiation power η. Dashed curve shows the radius in the case of linear propagation.

Conclusions

Thus, numerical simulation of propagation of a tightly focused high-power ultra-short laser pulse in air has shown that the process of formation of a focal waist has a dynamic character for such beams. This means that the spatial shape and the size of the waist (in both longitudinal and transversal directions) become dependent on the initial pulse power. Spatial focusing of the ultrashort laser pulse of even sub-critical power (for the process of the Kerr self-focusing) can lead to photoionization of the medium and plasma formation in the area with the maximal beam intensity, that will hinder the further growth of the wave intensity and transversal contraction of the beam as a whole. The higher is the pulse power, the more complex is the spatiotemporal structure of the focal waist, which is transformed from a spot, localized at a point, into an extended axial filament of variable diameter, consisting of many focal spots corresponding to individual time layers of the pulse.

Evolution of the rms beam size along the path is qualitatively similar to the behavior of linearly focused radiation, when a pronounced waist is formed at the point of the global focus. The difference of conditions of nonstationary focusing of a high-power pulse consists in the change of radiation divergence upon propagation through the global focus and in increase of the transversal dimension of the waist with increase of the pulse power.

The maximal degree of the beam intensity growth as a result of its geometric focusing decreases with the pulse power increase. From the viewpoint of the obtained extremely high values of the peak intensity (or energy density) at the global focus, the increase of the initial radiation power is inefficient, because the optical breakdown plasma, formed at the leading front of the pulse, blocks the focusing of the following time pulse layers.

Note that the results presented in this paper correspond to the situation of focused propagation of a high-power femtosecond laser radiation in atmospheric air and lie within the framework of the used model of medium photoionization (9). Application of other ionization model or study of laser pulse propagation in a different physical medium, having, for example, a higher atomic ionization potential may change quantitatively the estimates presented. In particular, there exist theoretical calculations[23] showing (with the model of a hydrogen atom taken as an example) that in superstrong optical fields ($\sim 10^{15}$ W/cm^2) the atom becomes resistant to ionization by radiation. This effect leads to a decrease of the photoionization rate with increase of the light wave intensity, which, in its turn, may restrict plasma formation in the region of the beam focus and remove obstacles for further growth of the radiation intensity.

References

1. C.B. Schaffer, A. Brodeur, J.F. Garca, and E. Mazur, Opt. Lett. **26**, 93–95 (2001).
2. K. König, I. Riemann, P. Fischer, and K. Halbhuber, Cell. and Mol. Biol. **45**, No. 2, 192–201 (1999).
3. W.R. Zipfel, R.M. Williams, R. Christie, A.Y. Nikitin, B.T. Hyman, and W.W. Webb, Proc. of the National Academy of Science (PNAS) **100**, No. 12, 7075–7080 (2003).
4. M.K. Grimes, A.R. Rundquist, J.-S. Lee, and M.C. Downer, Phys. Rev. Lett. **82**, No. 20, 4010–4013 (1999).
5. V.V. Bukin, N.S. Vorob'ev, S.V. Garnov, V.I. Konov, V.I. Lozovoi, A.A. Malyutin, M.Ya. Shchelev, and I.S. Yatskovskii, Quant. Electron. **36**, No. 7, 638–645 (2006).
6. M. Born and E. Wolf, *Principles of Optics* (Pergamon Press, 1959).
7. S.N. Vlasov and V.I. Talanov, *Self-Focusing of Waves* (Nizhnii Novgorod, 1997), 200 pp.
8. S.K. Turitsyn, V.K. Mezentsev, M. Dubov, A.M. Rubenchik, M.P. Fedoruk, and E.V. Podivilov, Opt. Express **15**, No. 22, 14750–14764 (2007).
9. Yu.P. Raizer, *Physics of Gas Discharge* (Nauka, Moscow, 1987), 592 pp.
10. V.N. Gol'dberg, V.I. Talanov, and R.E. Erm, Izv. Vyssh. Uchebn. Zaved., Radiofiz. **10**, No. 5, 674–685 (1967).

11. N. Akozbek, C.M. Bowden, A. Talebpour, and S.L. Chin, Phys. Rev. E **61**, No. 4, 4540–4549 (2000).
12. L. Berge, S. Skupin, R. Nuter, J. Kasparian, and J.-P. Wolf, Rep. Prog. Phys. **70**, 1633–1713 (2007).
13. V.P. Kandidov, O.G. Kosareva, E.I. Mozhaev, and M.P. Tamarov, Atmos. Oceanic Opt. **13**, No. 5, 394–401 (2000).
14. A.A. Zemlyanov and Yu.E. Geints, Atmos. Oceanic Opt. **20**, No. 1, 32–39 (2007).
15. A.M. Perelomov, V.S. Popov, and M.V. Terent'ev, Zh. Eksp. Teor. Fiz. **50**, 1393–1397 (1966).
16. A. Talebpour, J. Yang, and S.L. Chin, Opt. Commun. **163**, Nos. 1–3, 29–32 (1999).
17. S.N. Bagaev, Yu.E. Geints, A.A. Zemlyanov, A.M. Kabanov, G.G. Matvienko, E.V. Pestryakov, A.N. Stepanov, and V.I. Trunov, Atmos. Oceanic Opt. **20**, No. 5, 374–379 (2007).
18. A.A. Zemlyanov and Yu.E. Geints, Atmos. Oceanic Opt. **18**, No. 7, 514–519 (2005).
19. V.N. Lugovoi and A.M. Prokhorov, JETP Lett. **7**, No. 5, 117–119 (1968).
20. M.M.T. Lou and Y.R. Shen, Phys. Rev. Lett. **22**, No. 19, 994–997 (1969).
21. A. Brodeur, O.G. Kosareva, C.Y. Chien, F.A. Ilkov, V.P. Kandidov, and S.L. Chin, Opt. Lett. **22**, No. 5, 304–306 (1997).
22. H.R. Lange, G. Grillon, J.-F. Ripoche, M.A. Franco, B. Lamouroux, B.S. Prade, A. Mysyrowicz, E.T.J. Nibbering, and A. Chiron, Opt. Lett. **23**, No. 2, 120–122 (1998).
23. E.A. Volkova, A.M. Popov, and O.V. Tikhonova, Quant. Electron. **34**, No. 3, 216–222 (2004).